Chinese Journal of
POLYMER SCIENCE

RESEARCH ARTICLE

https://doi.org/10.1007/s10118-024-3088-6
Chinese J. Polym. Sci. **2024**, *42*, 739–750

Lightweight, Strong and High Heat-Resistant Poly(lactide acid) Foams *via* Microcellular Injection Molding with Self-Assembly Nucleating Agent

Xiao-Hu Bing[a,b], Wen-Yu Ma[b,c], Ming-Hui Wu[b], Peng Gao[b], Xiao Zhou[a,b], Hai-Bin Luo[b], Long Wang[b,c*], and Wen-Ge Zheng[b,c*]

[a] *School of materials Science and Engineering, Shanghai University, Shanghai 200444, China*
[b] *Ningbo Key Lab of Polymer Materials, Ningbo Institute of Material Technology and Engineering, Chinese Academy of Sciences, Ningbo 315201, China*
[c] *University of Chinese Academy of Sciences, Beijing 100049, China*

Abstract Poly(lactide acid) (PLA) foams have shown considerable promise as eco-friendly alternatives to nondegradable plastic foams, such as polystyrene (PS) foams. Nevertheless, PLA foam typically suffers from low heat-resistance and poor cellular structure stemming from its inherent slow crystallization rate and low melt strength. In this study, a high-performance PLA foam with well-defined cell morphology, exceptional strength and enhanced heat-resistance was successfully fabricated *via* a core-back microcellular injection molding (MIM) process. Differential scanning calorimetry (DSC) results revealed that the added hydrazine-based nucleating agent (HNA) significantly increased the crystallization temperature and accelerated the crystallization process of PLA. Remarkably, the addition of a 1.5 wt% of HNA led to a significant reduction in PLA's cell size, from 43.5 μm to 2.87 μm, and a remarkable increase in cell density, from 1.08×10^7 cells/cm^3 to 2.15×10^{10} cells/cm^3. This enhancement resulted in a final crystallinity of approximately 55.7% for the PLA blend foam, a marked improvement compared to the pure PLA foam. Furthermore, at 1.5 wt% HNA concentration, the tensile strength and tensile toughness of PLA blend foams demonstrated remarkable improvements of 136% and 463%, respectively. Additionally, the Vicat softening temperature of PLA blend foam increased significantly to 134.8 °C, whereas the pure PLA foam exhibited only about 59.7 °C. These findings underscore the potential for the preparation of lightweight injection-molded PLA foam with enhanced toughness and heat-resistance, which offers a viable approach for the production of high-performance PLA foams suitable for large-scale applications.

Keywords Poly(lactide acid); Nucleating agent; Microcellular injection molding; Heat-resistance; Toughness

Citation: Bing, X. H.; Ma, W. Y.; Wu, M. H.; Gao, P.; Zhou, X.; Luo, H. B.; Wang, L.; Zheng, W. G. Lightweight, strong and high heat-resistant poly(lactide acid) foams *via* microcellular injection molding with self-assembly nucleating agent. *Chinese J. Polym. Sci.* **2024**, *42*, 739–750.

INTRODUCTION

Microcellular polymeric foam refers to a polymer foam characterized by a cell density exceeding 10^9 cells/cm^3 and cell diameter smaller than 10 μm.[1] In comparison to conventional polymer foam, it offers the advantage of preserving mechanical strength to the greatest extent possible.[2] The techniques employed for the preparation of microcellular polymer foam encompass batch foaming, bead foaming, microcellular injection molding (MIM), and extrusion foaming. Among these, the MIM process using supercritical fluid stands out due to its distinctive attributes, including the capacity to fabricate products with higher precision and intricate geometries, reduced molding cycle times, and lower energy consumption.[3,4] Currently, intensive academic research and industrial applications are predominantly centered on petroleum-based polymer foams, most of them are non-biodegradable plastics that pose environmental pollution concerns. Consequently, there is an immediate and imperative need for comprehensive research efforts in the realm of bioplastics and biodegradable plastic foams, which could potentially relieve the serious environmental concerns associated with the prevalent use of petroleum-based polymer foams.[5]

Poly(lactic acid) (PLA), a biopolymer derived from renewable resources, possesses the distinctive property of rapid degradation under specific composting conditions.[6,7] The use of PLA offers a promising avenue for curtailing energy consumption and mitigating environmental pollution issues. Presently, several PLA products have been industrially manufactured for use as disposable plastics. In addition, PLA foam exhibits the potential to replace nondegradable plastics foams, such as polypropylene (PP), polyethylene (PE), and polystyrene (PS) in larger-scale applications, thanks to its high strength and high modulus.[8–10] Nonetheless, the fabrication of PLA foam through the MIM process faces substantial chal-

* Corresponding authors, E-mail: wanglong@nimte.ac.cn (L.W.)
E-mail: wgzheng@nimte.ac.cn (W.G.Z.)

Received November 17, 2023; Accepted December 25, 2023; Published online February 28, 2024

lenge arising from the inherent low melt strength of PLA. Several methods, including branching the long chains by reactive melt blending with chain extender,[11–13] incorporating particles, fibers[8,14–16] and controlling crystallization,[13,17,18] have been demonstrated to effectively enhance the melt strength and foaming ability of PLA.

Among these strategies, the controlling of crystallization has gained recognition as a straightforward and effective method for improving the foaming ability of PLA. Crystallization behavior imparts several benefits on the foaming process.[19] Firstly, the formed crystallization regions could efficiently provide numerous heterogeneous nucleation sites for cell formation. Secondly, the dissolution and diffusion of physical foaming agent would be restrained in the crystallization regions, leading to the creation of smaller cells around these regions. Thirdly, the crystals would impede the movement of molecular chains, acting as physical entanglement sites, thereby enhancing melt strength and restricting the overgrowth of cells. Consequently, controlling crystallization proves effective in managing the cell density, cell morphology and cell size in PLA foam preparation. To promote crystallization and accelerate the crystallization rate of PLA, adding appropriate nucleating agent is usually used as an effective method. In previous studies, various micro-/nano-particles have shown to effectively nucleate PLA crystallization, including talc,[20] modified montmorillonite,[21] kaolinite,[22,23] nanocellulose,[14,15,24,25] carbon nanotubes[26,27] and other inorganic powders. For instance, it was reported that the inclusion of cellulose nanofibers (CNFs) could efficiently improve the overall crystallization rate and the foaming behavior of PLA.[15,28] Additionally, the addition of modified CNFs could enhance the mechanical strength of foamed PLA due to the refined cellular morphology and the reinforcing effect of CNFs.[14] However, the utilization of nanofillers typically encounters the challenge of dispersion within the polymer matrix, with inadequate dispersion often leading to reduced nucleation efficiency. Furthermore, selecting a suitable nanoparticle can be complex due to the distinct promotion effects exhibited by different fillers on PLA foaming behaviors.

Recently, researches showed that specialized crystal nucleating agents, including amide-based,[29,30] hydrazide-based,[31–33] and other self-assembly nucleating agent,[34] exhibited high efficiency in controlling the crystallization of PLA. In contrast to the use of inorganic/organic nanoparticles, hydrazide-based nucleating agent (HNA) can dissolve within the PLA melt and achieve optimal dispersion in PLA matrix. It indicated that the imino group within HNA could engage in dipole-dipole interactions with the carbonyl group in PLA, leading to conformational alterations in PLA molecular chains.[35,36] Consequently, PLA can initiate crystal formation on the surface of self-assembled nucleating agent fibers with a lower energy barrier. However, there are exceedingly few reports exploring the enhancement of PLA's foaming ability through the incorporation of self-assembled nucleating agent.[30,31] For instance, Tang *et al*.[12] observed that the cell size of branched PLA foam adding with HNA could be reduced to 10 μm. Similarly, Wu *et al*.[19] improved the crystallization of PLA using the self-assembly crystal nucleating agent TMC-306, resulting in a reduction in foam cell size from 50 μm to a mere 360 nm, but limited the expansion ratio. However, it is essential to emphasize that these studies primarily concentrated on PLA foams fabricated through batch foaming process, and comprehensive investigations into the mechanical properties and heat resistance of PLA foams remain relatively unexplored.

In this study, we successfully prepared PLA foam products with excellent heat resistance, well-defined cell structure and high performance, which was achieved through the incorporation of a hydrazide-based nucleating agent (HNA), specifically TMC-300, and the utilization of supercritical nitrogen as a physical foaming agent, combined with a core-back MIM process. Firstly, the crystallization behavior and complex viscosity of PLA/HNA blends were investigated employing differential scanning calorimetry (DSC) and rotational rheology tests. Subsequently, the effects of varying HNA contents and diverse holding pressures on the cell structure and crystallinity of the prepared microcellular foams were studied. Lastly, the tensile properties and heat resistance of the fabricated microcellular foams were assessed. This study provides a straightforward and efficient approach for advancing the development and utilization of high-performance PLA foam in industrial applications.

EXPERIMENTAL

Materials

Commercial PLA, designated as FY601, was provided by Anhui BBCA Biochemical & Futerro PLA Co., Ltd, China, possesses a D-lactic acid content of less than 1%. Its number- and weight-average molecular weights were 0.95×10^5 and 1.44×10^5 g·mol^{-1}, respectively. It displays a melt flow rate of 9.0 g/10min (190 °C/2.16 kg). The self-assemble nucleating agent, TMC-300, was purchased from Shanxi Provincial Institute of the Chemical Industry, China. The physical blowing agent, N_2 (99% purity), was obtained from Ningbo Huayu Gas Inc, China. The chemical structures of moleculars are shown in Fig. 1.

Blends Preparation

A co-rotational twin-screw extruder (AK 36, Nanjing KY Chemical Machinery Co., Ltd, China) was employed to prepare the PLA/HNA blends. The length/diameter ratio and screw diameter of the extruder were 44 and 36 mm, respectively. The temperatures from hopper to die were set to be from 165 °C to 185 °C. The extrusion process maintained a discharge rate of 15 kg/h and a screw speed of 45 r/min. A master batch of PLA with 3

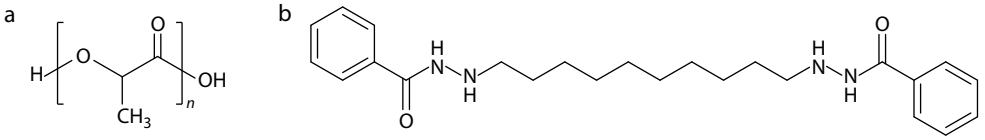

Fig. 1 Chemical structures of (a) PLA and (b) TMC-300.

https://doi.org/10.1007/s10118-024-3088-6

wt% HNA was first produced through melt blending and then the master batch was diluted with neat PLA to prepare PLA blends with varying nucleating agent content: 0.5 wt%, 1.0 wt% and 1.5 wt%. For convenience, PLA blends with different contents of nucleating agent were designated as PLA-*x*, where '*x*' denotes the weight percentage of HNA incorporated into the PLA matrix. For instance, PLA-1.5 indicated the addition of 1.5 wt% HNA within the PLA matrix. It is noted that PLA resin was dried at 80 °C for 4 h before compounding and after pelletizing for the next step experiments.

Core-back Microcellular Injection Molding (MIM) Process

A 100-ton injection molding machine (Systec 100/420-310C, Demag Plastics Group, Germany) equipped with a 35-mm diameter screw, along with a MuCell supercritical fluid delivery system (T100, Trexel Inc., USA) was employed to conduct the core-back MIM experiments. In contrast to conventional foam injection molding (FIM), one of the key features of the core-back MIM technology is that the filling and foaming processes are separated. In the core-back MIM process, the steps are as follows. Initially, the supercritical N_2 is dissolved into the polymer melt within the heated cylinder, resulting in the formation of a homogeneous polymer/gas mixture before injection processing. Subsequently, part of the dissolved gas would undergo cell nucleate and grow due to the pressure drop at the gate during the filling stage. During the dwelling stage of core-back MIM, cells could resolve back into the matrix with appropriate packing pressure and packing time. The subsequent core-back (mold-opening) process ensures uniform pressure reduction within the mold, facilitating the homogeneous foaming process.[37] In this experiment, a standard tensile testing mold (GB/T 1040) with a thickness of 3 mm was used. It is noteworthy that the void fraction of the MIM foams was consistently maintained at 25%. The melt and mold temperatures were set to be 195 and 70 °C, respectively. The packing pressure and packing time were carefully set within an appropriate range based on a series of pilot tests. Table 1 shows the detailed processing conditions in this experiment.

Table 1 Processing parameters used in the core-back MIM process.

Processing parameters	Value
Melt temperature (°C)	195
Mold temperature (°C)	70
Injection speed (mm/s)	100
Packing pressure (MPa)	40
Packing time (s)	16, 18, 22
Cooling time (s)	60
Mold-opening distance (mm)	1
N_2 dosage (wt%)	0.8

Thermal Analysis

A differential scanning calorimetry (DSC) DSC3+ manufactured by Mettler Toledo Inc., was used to characterize the non-isothermal crystallization behaviors of neat PLA and PLA/HNA blends under a nitrogen atmosphere with a flow rate of 20 mL/min. Samples weighing approximately 6 mg to 8 mg were cut from both solid samples and foamed specimens. The samples were first heated to 200 °C, isothermally held at 200 °C for 5 min to remove the residual thermal histories, subsequently cooled to 25 °C at a cooling rate of 10 °C/min, and finally reheated them to 200 °C to obtain melting curves.

The crystallinity of the PLA (X_c) can be obtained using the following Eq. (1):

$$X_c = \frac{\Delta H_m - \Delta H_c}{\varphi \Delta H_m^0} \quad (1)$$

where ΔH_m, ΔH_c, φ and ΔH_m^0 are the melting enthalpy, the cold crystallization enthalpy, the weight fraction of PLA and the melting enthalpy of a perfectly crystalline PLLA, respectively. The ΔH_m^0 for 100% crystallites of PLLA was selected as 93.6 J/g.

Dynamic Rheological Test

Rheological behaviors of the neat PLA and PLA/HNA blends were measured with an ARES rotational rheometer (HR-3, TA, USA). The testing specimens with a diameter of 25 mm and thickness of 1 mm were prepared by a hot press at 10 MPa and 190 °C for 10 min. The temperature sweep was performed in the temperature range of 80–190 °C at 1 rad/s, with a fixed strain of 1%. Then, the frequency sweep was performed in the frequency range of 0.01–100 rad/s at a temperature of 190 °C, with a strain of 1%.

Foam Morphology Characterization

A scanning electron microscope (SEM) (EVO 18, Zeiss Group, Germany) was employed to investigate the microstructures of injection-molded foams at a voltage of 20 kV. The specimens underwent cryogenic treatment in liquid nitrogen for 30 min, and then were cryogenically fractured perpendicular to the mold opening direction. Prior to observation, the surface of the specimens was coated with a thin layer of platinum.

The average cell size and cell density were determined based on the SEM micrographs. The number-averaged cell diameter (d) was calculated using Eq. (2):

$$d = \frac{\sum d_i n_i}{\sum n_i} \quad (2)$$

where n_i is the number of bubbles with a dimeter of d_i, assuming a spherical bubble shape. The cell nucleation density (N_0) was calculated using Eq. (3):

$$N_0 = \left(\frac{n}{A}\right)^{3/2} \frac{\rho_p}{\rho_f} \quad (3)$$

where n is the number of bubbles, A represents the area of the SEM micrograph, ρ_p and ρ_f denote the density of the solid specimens and the foam, respectively. These densities were determined using a water displacement method.

Crystal Morphology Characterization

The crystal morphologies were assessed using a SEM (S-4800, Hitachi, Japan) operating at 4 kV. Small specimens, obtained by cutting sections perpendicular or parallel to the flow direction of the injection-molded samples, were cryogenically fractured in liquid nitrogen. Subsequently, the fracture surface was etched with a water-methanol-sodium hydroxide mixture solution (13 mL:27 mL:40 mg) for 12 h at 25 °C.[36] Prior to SEM observation, the specimen surfaces were sputtered a layer of platinum.

Mechanical Properties

Tensile testing of PLA specimens was carried out using a tensile testing equipment (Instron 5567, Instron, USA) in accordance with GB/T 1040.2-2006. The crosshead speed was set to 50

mm/min, and the reported values represent the average of multiple tests.

Heat Resistance Test

The heat resistance properties of the neat PLA and PLA/HNA blend foams were evaluated using the Vicat softening temperature (VST) testing method, in accordance with GB/T1633-2000. Specimens were extracted from the injection-molded part. The testing specimens were placed on the test bench and the piercing needle was rested on the surface at least 1 mm from the edge. The specimen was then immersed in a silicone oil bath with a load of 10 N for 10 min. Subsequently, the oil temperature was increased at a rate of 120 °C/h until the piercing needle penetrated the specimen by 1 mm.

RESULTS AND DISCUSSION

Thermal Behaviors

Figs. 2(a) and 2(b) illustrate the non-isothermal crystallization curves for both neat PLA and PLA/HNA blends, which were recorded during the first cooling and the second heating stages, respectively. As depicted in Fig. 2(a), it could be observed that the crystallization peak temperature, T_c, of PLA blends with a nucleating agent content exceeding 0.5 wt% is much higher than that of neat PLA. Table 2 shows that the specific T_c values of the PLA-0.5, PLA-1.0, PLA-1.5, PLA-3.0 and neat PLA, registering at 105.9, 117.7, 126.2, 130.9 and 98.3 °C, respectively. Notably, PLA-3.0 specimen exhibits a remarkable T_c elevation of 32.6 °C compares to the neat PLA, revealing that the added nucleating agent could effectively improve the crystallization capacity of PLA. Furthermore, it is noteworthy that PLA-3.0 specimen displays a distinct cold crystallization peak at approximately 156 °C, attributed to the crystallization of the self-assembled nucleating agent.[36] As shown in Fig. 2(b), it can be observed that the cold crystallization peak temperature, T_{cc}, of PLA-0.5 reduces from 100.7 °C to 88.5 °C, while the degree of crystallinity (X_c) increases from 26.2% to 45.8%. This change underscored the pronounced nucleating effect of HNA in PLA. Moreover, as the content of HNA increases from 0.5 wt% to 3.0 wt%, the X_c of PLA/HNA blends slightly increased from 45.8% to 50.8%.

Rheological Behaviors

Fig. 3(a) presents the complex viscosity (η^*) of neat PLA and PLA/HNA blends over a temperature range of 200–100 °C. This revealed that the complex viscosity of PLA exhibited a linear increase with temperature from 200 °C to 120 °C. An abrupt increase in viscosity was observed for PLA at about 120 °C, which was attributed to the onset crystallization of PLA. Compared with the neat PLA, the addition of HNA significantly increased the onset crystallization temperature. Moreover, with the increasing of HNA content, the temperature corresponding to the sharp viscosity increase rise gradually shifted, reflecting the heightened crystallization temperature achieved. Intriguingly, for HNA contents exceeding 1.0 wt%, the two steps increment of complex viscosity emerged. Specifically, in the case of PLA-1.5, the initial viscosity increment appeared at 150 °C, followed by a secondary increment occurring in the vicinity of 140 °C. That phenomenon arises from the differential crystallization of a higher proportion of TMC-300 from the PLA/HNA blends, occurring prior to the initiation of PLA crystallization during the cooling process. Additionally, Fig. 3(b) displays the complex viscosity curve as a function of frequency for PLA/HNA blends at a temperature of 190 °C. Generally, it illustrated that the addition of HNA could enhance the melt strength of PLA. That was due to propensity of the self-assembled nucleating agent, when separated from the PLA melt, could form a network framework.[38,39] Consequently, this network structures restricted the free movement of polymer molecular chains within the blend.[39] Notably, in comparison to other blends, PLA-3.0 specimen exhibites a substantial enhancement in complex viscosity

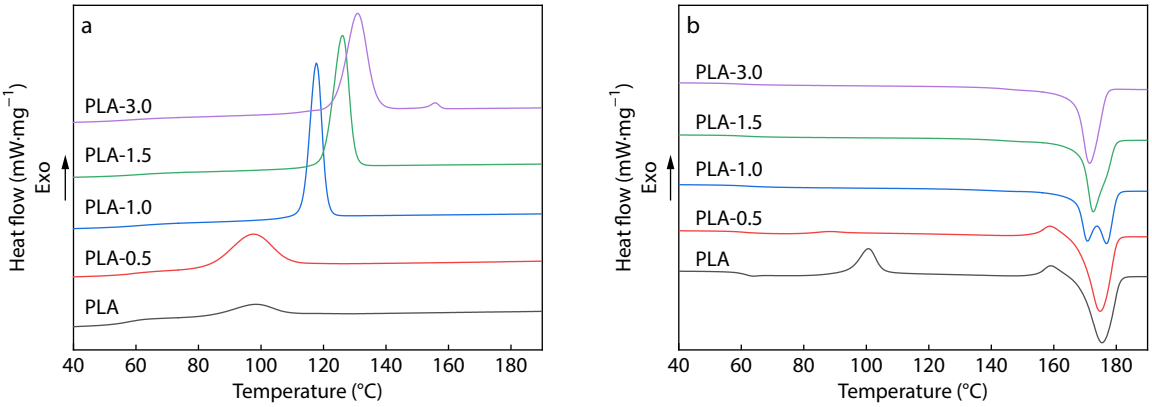

Fig. 2 DSC curves of PLA blends with different contents of TMC-300: (a) the first cooling runs from the melt to room temperature at a rate of 10 °C/min, and (b) the second heating runs to 200 °C at a rate of 10 °C/min.

Table 2 Thermal parameters of PLA/HNA blends obtained from DSC curves.

Sample	T_c (°C)	T_{cc} (°C)	X_{cc} (%)	T_m (°C)	X_m (%)	X_c (%)
PLA	98.3	100.7	18.3	175.4	44.5	26.2
PLA-0.5	105.9	88.5	3.2	174.8	49.0	45.8
PLA-1.0	117.7	/	/	170.8, 176.8	49.5	49.5
PLA-1.5	126.2	/	/	172.3	49.5	49.5
PLA-3.0	130.9	/	/	171.5	50.8	50.8

https://doi.org/10.1007/s10118-024-3088-6

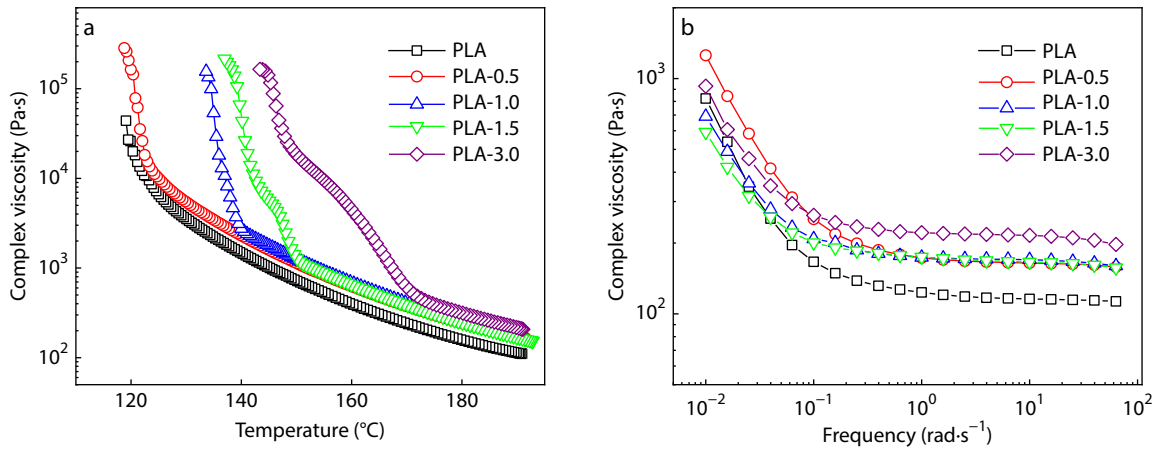

Fig. 3 Complex viscosity (η^*) of neat PLA and PLA/HNA blends measured as a function of (a) temperature and (b) frequency.

within the higher frequency range.

Effect of HNA on Cellular Morphologies

Fig. 4 shows the SEM micrographs of PLA/HNA blends foams with different content of nucleating agent prepared under an optimized packing time of 22 s. In general, the neat PLA foam prepared by MIM process with core-back technology usually exhibited a relatively poor morphology, which could be found in Fig. 4(a). In contrast, with the introduction of self-assembled nucleating agent, much finer cellular structures were achieved for the PLA/HNA blends. Furthermore, with the increase of nucleating agent content, cell density of the core layer of PLA blends foams gradually increased. Especially, as demonstrated in Figs. 5(a) and 5(b), the cell densities for PLA-1.5 and PLA-3.0 foams increase significantly to 2.15×10^{10} and 5.90×10^{10} cells/cm^3, respectively. Meanwhile, a significant reduction in cell size was evident in PLA/HNA blends foams. Specifically, the corresponding average cell diameter decreased from 43.5 μm to 2.67 μm. These results clearly indicated that the addition of HNA could significantly improve the foaming behavior of PLA. This improvement in foaming process was probably attributed to the provision of a greater number of heterogeneous cell nucleation sites at elevated nucleating agent contents, predominantly at the interface between crystalline and amorphous regions.[13] Additionally, the subsequent cell growth process is another crucial step for the final cell structures, in addition to cell nucleation. The cell growth is closely related to the extensional flow behavior of the polymer/gas mixture.[40,41] Therefore, the increased presence of microcrystals results in higher melt viscosity, which hinders cell coalescence and the expansion of cell walls, ultimately leading to smaller cell sizes.

Furthermore, the influence of packing time on cell structure was studied. Packing time is the time when polymer melt experiences from the beginning of injection to the foaming process.[13] In these experiments, we selected a relatively long packing time to serve a dual purpose: not only did it facilitate the effective re-dissolution of the gate-nucleated bubbles,

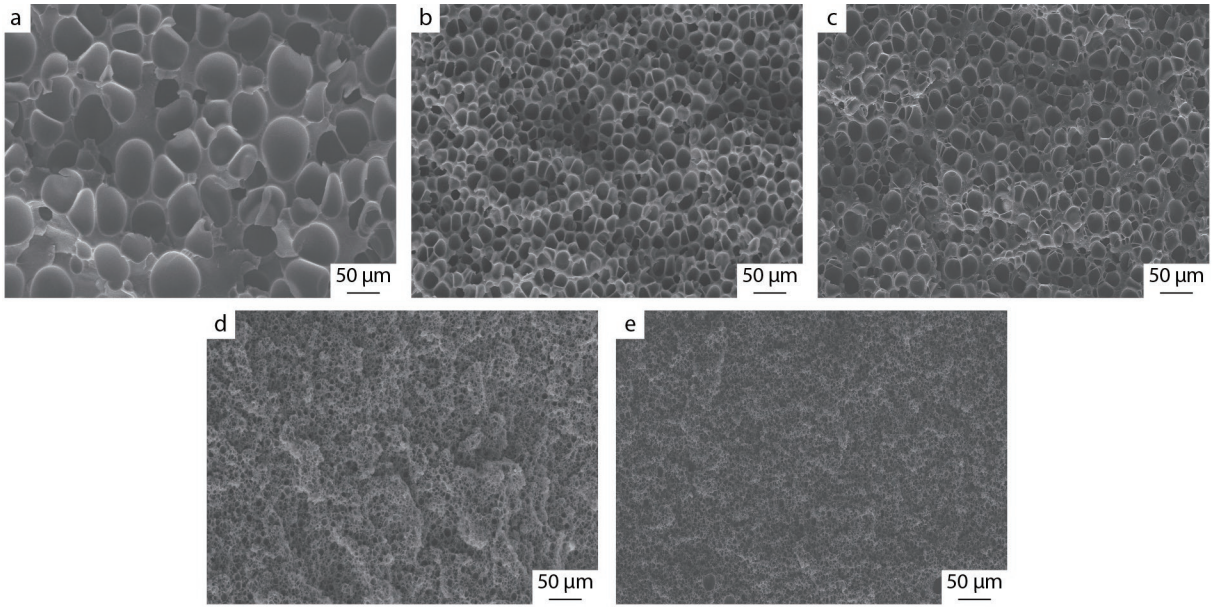

Fig. 4 SEM micrographs of PLA/HNA blend foams fabricated at a packing time of 22 s: (a) PLA, (b) PLA-0.5, (c) PLA-1.0, (d) PLA-1.5, and (e) PLA-3.0.

https://doi.org/10.1007/s10118-024-3088-6

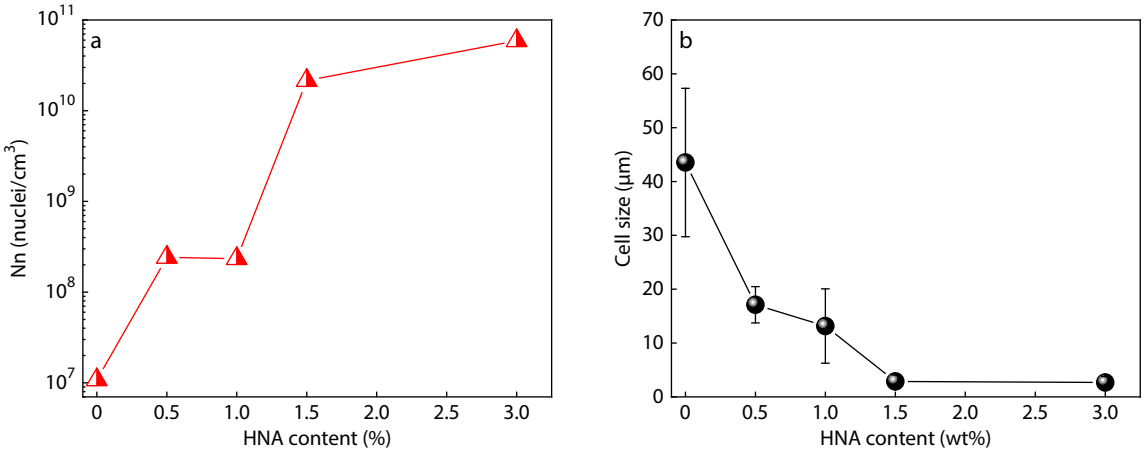

Fig. 5 Variation in (a) cell density and (b) average cell diameter as a function of HNA content for PLA/HNA blend foams fabricated at a fix packing time of 22 s.

but it also reflected the influence of PLA crystallization nucleation rates on cell morphology. Fig. 6 shows the SEM micrographs illustrating the cell morphologies of both neat PLA and PLA-1.5 foams. These foams were fabricated under the conditions of packing pressure of 40 MPa, while varying the packing time between 16, 18 and 22 s, respectively. As shown in Figs. 6(a)–6(c) and 7, neat PLA foams, regardless of packing times, consistently displayed a notable larger cell size and lower cell density, with negligible alterations in the overall cell morphology. This could be resulting from that the crystallization nucleation rate of neat PLA was so slow that the crystallization did not change significantly within the setting time. Conversely, as revealed in Figs. 6(d)–6(f) and 7, by prolonging the packing time from 16 s to 22 s, the cell density of PLA-1.5 foam exhibited a remarkable two-order-of-magnitude increase in cell density, accompanied by an 83.6% reduction in the average cell diameter. This notable transformation was closely related to the expedited crystallization nucleation rate of PLA-1.5.

Crystalline Structures of PLA/HNA Blends

Figs. 8(a)–8(c) show the first heating curves and the corresponding crystallinity results for the injection-molded solid PLA blends and their foams with different nucleating agent contents. The solid PLA/HNA blends were prepared under the same heating condition as the foams, resulting in a discernible reduction in the cold crystallization peak temperatures (T_{cc}) from 100.8 °C to 85.6 °C. This observation indicated that the amorphous phase within the solid PLA/HNA blends tended to form a pre-ordered structure with the increasing of TMC-300 content. In contrast, the PLA/HNA blend foams prepared by MIM process not only exhibit reduced cold crystallization peak temperature, but also display a reduction in the area of the cold crystallization peak on the curve. For instance, the cold crystallization

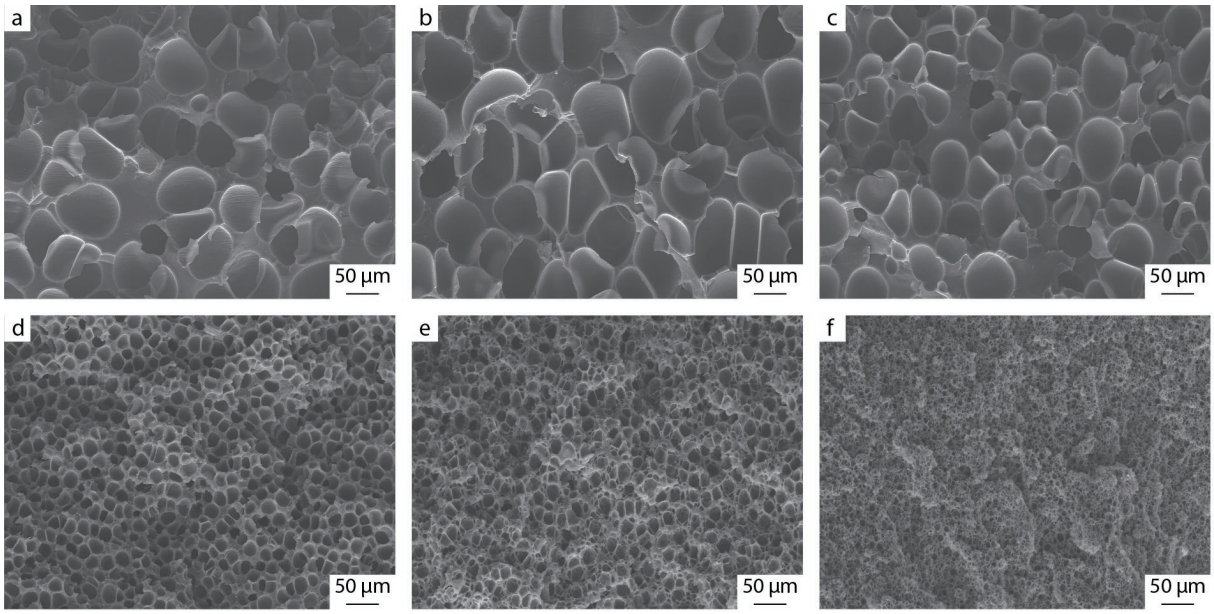

Fig. 6 SEM micrographs of neat PLA foam (a–c) and PLA-1.5 foam (d–f) fabricated using different packing time: (a, d) 16 s, (b, e) 18 s, and (c, f) 22 s.

https://doi.org/10.1007/s10118-024-3088-6

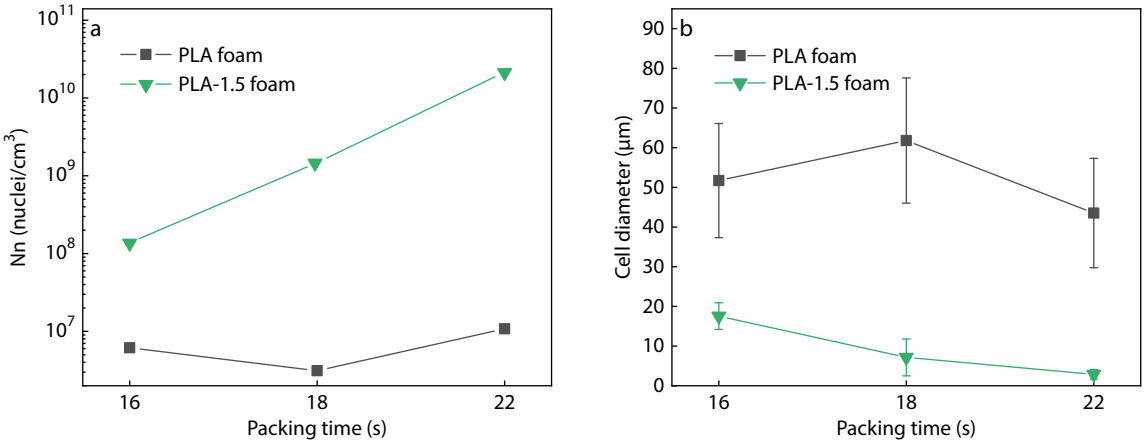

Fig. 7 Variation in (a) cell density and (b) average cell diameter with different packing time for neat PLA and PLA-1.5 foams.

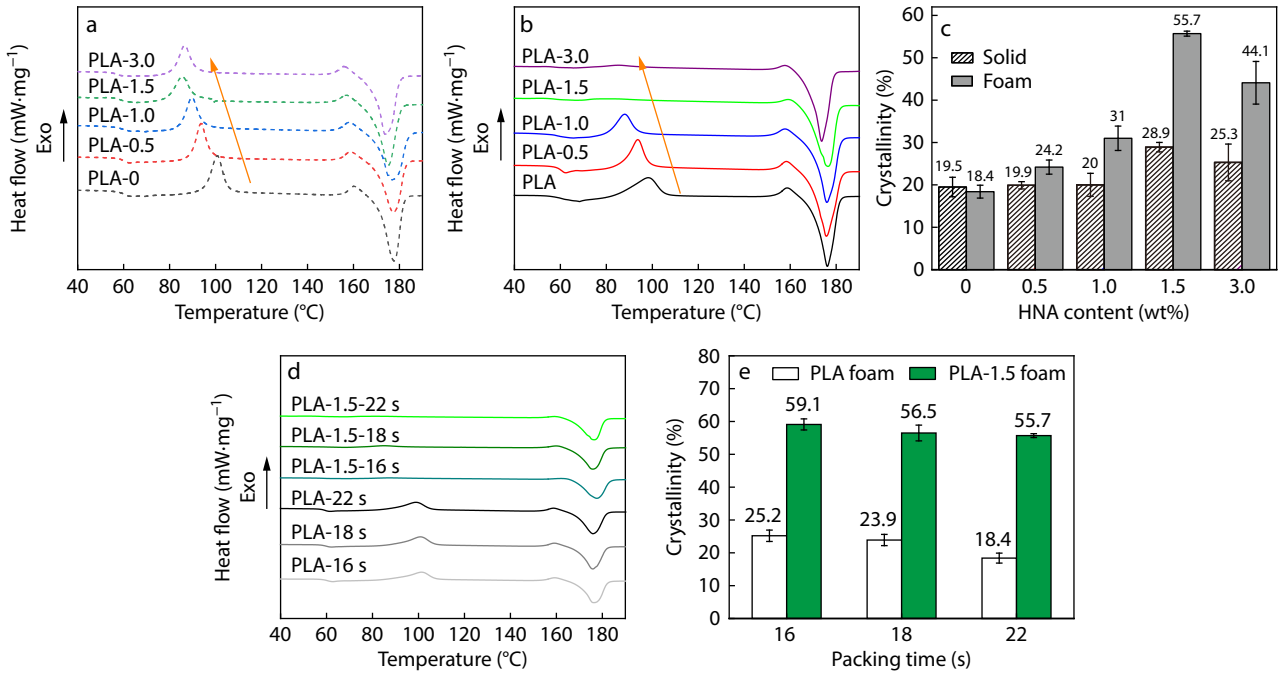

Fig. 8 DSC curves of non-isothermal behavior of PLA blends with varying HNA: (a) solid specimens, (b) foams, and (c) crystallinity for both solid and foamed samples fabricated at a packing time of 22 s; (d) DSC curves of non-isothermal behavior, and (e) crystallinity of neat PLA and PLA-1.5 foams under different packing time.

peak almost disappeared for the PLA-1.5 foam, ultimately resulting in a crystallinity of approximately 56%. These findings revealed that a higher nucleating agent content not only augmented crystallization capacity of PLA but also enhanced the foaming capacity of PLA. Specifically, during the cell growth process, the biaxial stretching behavior exerted upon the surrounding cell walls would improve the orientation of molecular chains, thereby promoting PLA crystallization.[42,43] However, in comparison to PLA-1.5 foam, the crystallinity of PLA-3.0 foam decreased. Although the increase of nucleating agent content could greatly promote PLA crystal nucleation, excessive content would lead to nucleating agent accumulation during the precipitation process, impeding the growth of PLA crystals and eventually resulting in a decrease in crystallinity.

Figs. 8(d) and 8(e) display the first heating curve and crystallinity results for the pure PLA foam and PLA-1.5 foam prepared under different packing time. It was illustrated that with the increase in packing time, the crystallinity both of the foams decreased slightly. It could be attributed to the fact that PLA crystal nucleation could be promoted and the growth could be impeded, resulting a lower crystallinity for a longer packing time.

Furthermore, the injection-molded PLA/HNA blends were etched to remove the HNA and the amorphous regions of PLA matrix, and the cross-section perpendicular to the flow direction was observed, as shown in Fig. 9. Fig. 9(a) reveals that the neat injection-molded PLA did not form a complete spherulite structure. Similarly, both PLA-0.5 and PLA-1.0 blends only exhibit holes created by the removal of TMC-300 fibers and the crystal morphology could not be observed, re-

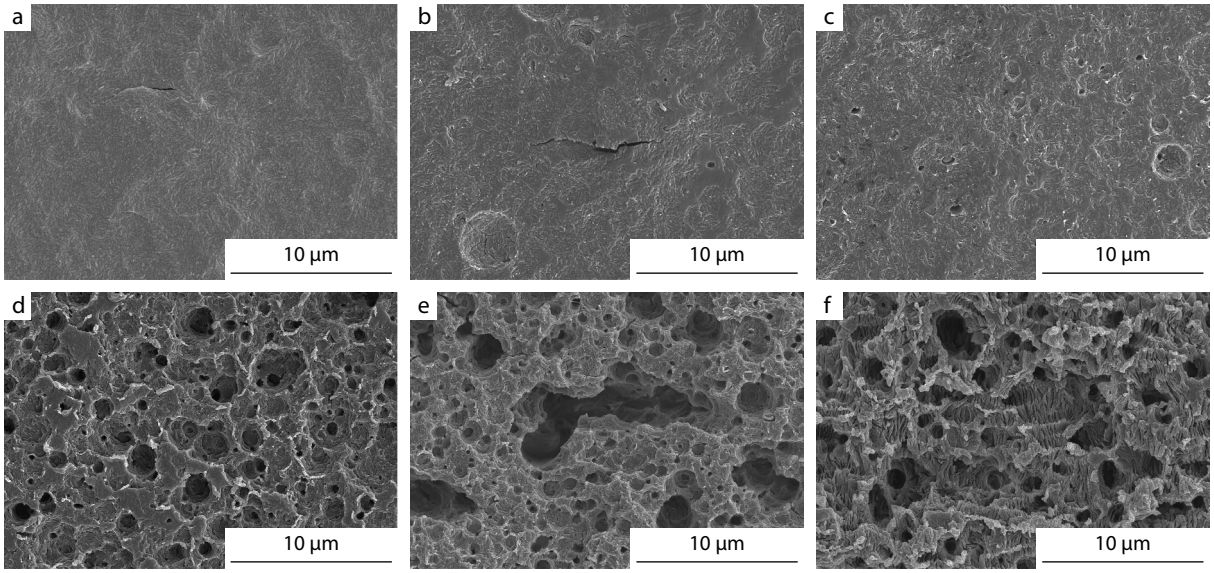

Fig. 9 SEM micrographs of PLA/HNA blends containing different HNA contents: (a) neat PLA, (b) PLA-0.5, (c) PLA-1.0, (d) PLA-1.5, (e) PLA-3.0, and (f) annealed PLA-1.5.

sulting from the lower crystallization ability. In contrast, PLA-1.5 and PLA-3.0 blends display a notable retention of numerous voids on the etched surface due to their elevated crystallization capacity and crystallinity. It was noteworthy that nucleating agents within the PLA-1.5 blend were uniformly distributed in the PLA matrix, whereas nucleating agents in PLA-3.0 accumulat during the precipitation process, which would significantly affect the subsequent mechanical properties of the material. According to the DSC results discussed in the previous section, the crystallinity of injection-molded PLA products could be enhanced with the increase of nucleating agent content, yet the crystallinity of solid samples prepared directly through injection molding was at a low level. Consequently, a relatively clear crystal structure could not be observed after etching the nucleating agent and amorphous regions. To address this, the prepared samples were annealed to further refine their crystal structure and then treated under uniform etching conditions. The outcomes are presented in Fig. 9(f). In comparison to the incompletely crystallized PLA-1.5 sample, the annealed specimen revealed a more complete crystal structure, showing clear crystal morphology of lamellar string arrangement surrounding the etched TMC-300. This result indicated that suitable etching conditions were applied in this experiment context. Moreover, due to the orientation of the precipitated fibrous nucleating agent related to the flow field during the injection process, the observed cavity was mostly in the shape of depth.[31]

Tensile Properties of PLA/HNA Blend Foams

Typically, the injection-molded polymeric foam consists of a solid skin layer and the foamed core-layer, with the foamed core layer being the dominant portions within the specimen. The core layer of microcellular injection-molded foams usually exhibited distinct mechanical characteristics compared to the outer solid skin layers.[9] To explore the influence of cell structure and crystallization on the mechanical property of PLA foams, we removed the skin layer surrounding the foams while preserving the core layer, which maintained uniform cell structure for subsequent testing. Fig. 10 presents the tensile mechanical properties and the typical stress-strain curves for PLA foams with different nucleating agent contents, with the skin layer intentionally removed. Compare with the pure PLA foam, the tensile modulus of PLA blend foams increased obviously with the addition of HNA. Specifically, the inclusion of 1.5 wt% HNA led to a remarkable 93% enhancement in the tensile modulus of PLA foam. This enhancement could be primarily attributed to the higher crystallinity for the PLA blend foam, as higher crystallinity always corresponded to a higher tensile modulus. Furthermore, in comparison to the pure PLA foam, the tensile strength of the PLA blend foam with the introduction of 1.5 wt% HNA experienced a notable 136% increase. It can be found that the trends in tensile strength of foams are positively related to the enhanced crystallization and the refined cell morphology with different content nucleating agent. PLA foams characterized by smaller cell size and higher cell densities tended to display superior tensile strength. Fig. 10(c) shows the tensile toughness of PLA/HNA blend foams. Notably, compare with the pure PLA foam, the tensile toughness of PLA-1.5 foam is significantly increased by 463%, particularly when PLA-1.5 foam has a crystallinity of about 56%. This significant enhancement could be attributed to the presence of more uniform and fine cell structures, as well as uniform nucleating agent dispersion, both of which played pivotal roles in the toughening of PLA.[14,31] However, an excessive content of nucleating agent led to a reduction in tensile toughness, primarily attributed to stress concentration caused by the aggregation of the nucleating agent.

Fig. 11 shows the tensile properties of PLA blend foams with different packing time. As discussed in Section **Crystalline Structures of PLA/HNA Blends**, PLA foams prepared with the same HNA content but different packing time exhibited little changes in crystallinity. Consequently, the observed differences in the subsequent part of the test primarily arose from variations in the cell structure. Fig. 11 illustrates that under different packing time, neat PLA foam exhibited relatively low and largely insignificant changes in tensile strength and

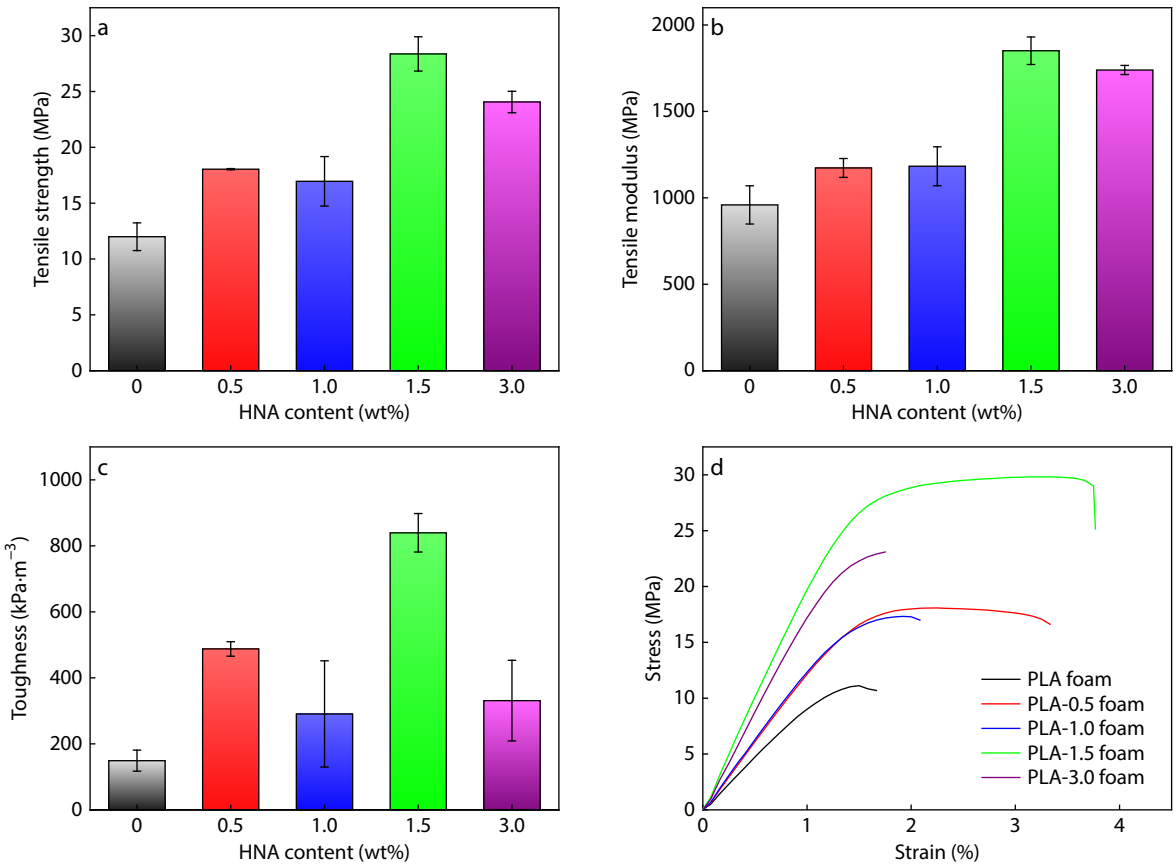

Fig. 10 Tensile properties of PLA/HNA blend foams with different nucleating agent contents: (a) tensile strength, (b) tensile modulus, (c) toughness, and (d) stress-strain curves.

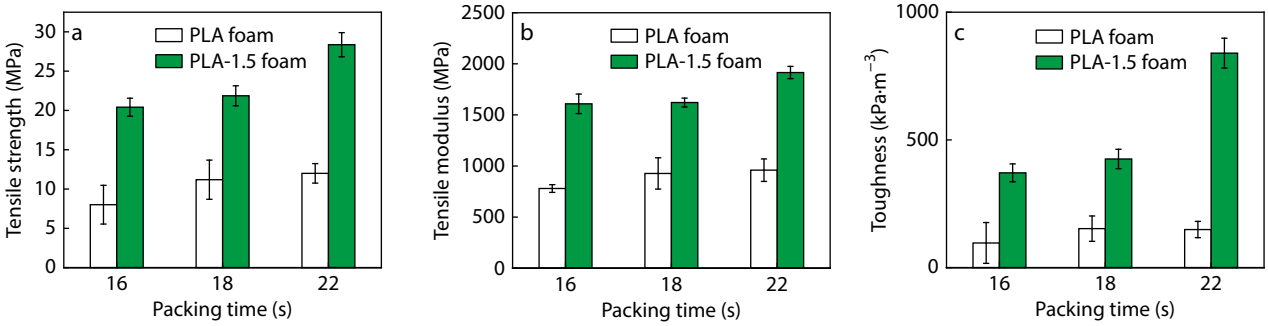

Fig. 11 Tensile properties of neat PLA and PLA-1.5 foams with different packing time: (a) tensile strength, (b) tensile modulus, and (c) toughness.

modulus. Conversely, in the case of PLA-1.5 foam, an extended packing time led to a significant enhancement in tensile strength, tensile modulus, and toughness by 39%, 19% and 126%, respectively. This enhancement could be attributed to the conspicuous improvement in cell morphology within the PLA-1.5 foam compared to the neat PLA foam. It was indicated that the reduction in cell size and the increase in cell density contributed to a more uniform distribution of stress within the material under tension, thereby mitigating the stress concentration resulting from larger cells.

Heat Resistance of PLA/HNA Foams

Neat PLA, fabricated through common thermoplastic processing methods such as injection molding and extrusion, typically exhibits poor heat resistance, which seriously constrains the application range of PLA. This limitation arises from the inherently low crystallinity of PLA foams. Moreover, conventional annealing process tend to distort and expand the structural integrity of PLA foam, primarily due to the secondary foaming process of bubbles at a high-temperature atmosphere.[44] In the present experiment, injection-molded PLA/HNA blend foams with high heat resistance were successfully prepared directly using the MIM with the core-back operation. The heat resistance related results are depicted in Fig. 12. Comparatively, PLA-1.5 foam exhibits a substantial improvement in average Vicat softening temperature (VST), increasing from 59.7 °C to 134.8 °C when compared to neat PLA foam. However, PLA blend foams containing less than 1.5 wt% content of TMC-300 display only

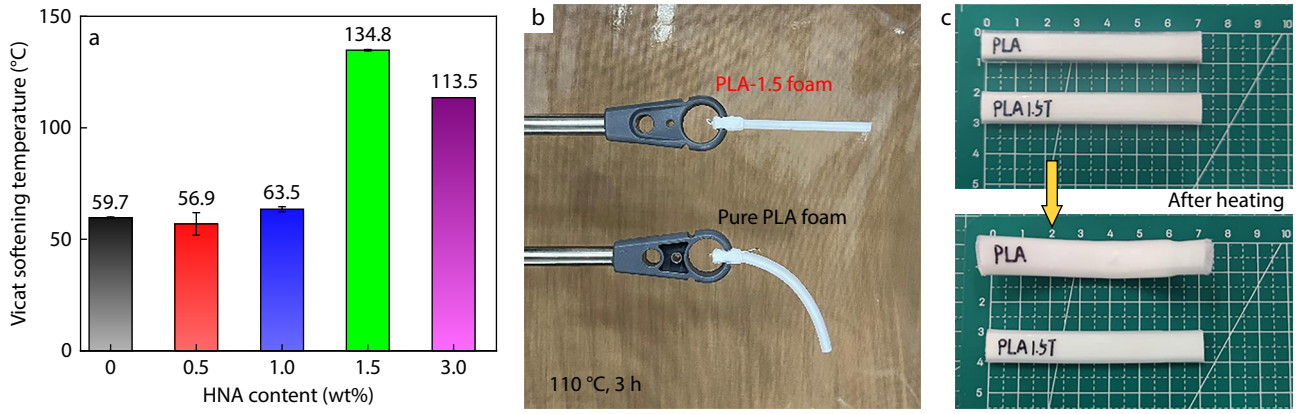

Fig. 12 (a) VST testing results of PLA blend foams, (b) digital photographs during the thermal deformation process of pure PLA and PLA-1.5 foams treated at 110 °C for 3 h, and (c) size changes before and after the thermal deformation process.

marginal deviations from the heat resistance of PLA foam. That phenomenon was attributed to that the heat resistance of PLA was often positively correlated with its crystallinity. It should be noted that significant enhancements in heat resistance were typically observed when crystallinity surpassed a critical threshold.[45]

The VST serves as a valuable indicator for assessing the shape stability of polymers when subjected at elevated temperatures.[46] Consequently, we conducted an experiment involving the PLA-1.5 foam and the pure PLA foam by subjecting them to an oven at 110 °C to observe the evolution of shape and structure, as shown in Figs. 12(b) and 12(c). The observations show a marked distinction between the two materials. It revealed that the neat PLA foam exhibited rapid bending and deformation upon heating, while the structure and shape of the PLA-1.5 foam remained remarkably unchanged. Further analysis of the size changes before and after the thermal deformation process displayed that the dimensions of the PLA-1.5 foam samples remained unaffected at 110 °C. This implied that the prepared injection-molded PLA/HNA blend foams possess the capability to undergo high-temperature annealing treatments while maintaining their structural integrity.

CONCLUSIONS

In this study, PLA foams with well-defined cell structure, excellent mechanical properties, and thermal stability were successfully prepared with the incorporation of the self-assembled nucleating agent HNA using core-back microcellular injection molding process. Differential scanning calorimetry results demonstrated that the added HNA significantly increased the crystallization temperature and crystallization rate of PLA. Consequently, the crystallization process leads to a marked rise in PLA viscosity, effectively preventing cell coalescence and restricting cell growth. Notably, when the HNA content exceeded 1.5 wt%, the final PLA foam exhibited an impressive cell density exceeding 10^{10} cells/cm^3 and an average cell diameter below 3 μm. Furthermore, we observed a direct correlation between the cell structure of PLA-1.5 foam and the packing pressure time. The foaming process additionally enhanced the crystallization of PLA. The as-prepared PLA-1.5 foam exhibited a remarkable crystallinity of 56%, as opposed to 37% and 27% exhibited by neat PLA foam and solid PLA-1.5 blends, respectively. Tensile results revealed that significant enhancements, with approximately 136% and 463% improvements in tensile strength and toughness, respectively, for PLA-1.5 foam when compared to neat PLA foam. These notable improvements could be attributed to the blend foam's high crystallinity, well-defined cell structure, and effective dispersion of nucleating agent fibers. Moreover, the Vicat softening temperature of PLA-1.5 foam reached an impressive 134.8 °C, approximately 75 °C higher than that of pure PLA foam, demonstrating its resistance to deformation even at temperatures as high as 110 °C. Therefore, this work offers a viable approach for the production of high-performance PLA foams.

Conflict of Interests

The authors declare no interest conflict.

Data Availability Statement

The data that support the findings of this study are available from the corresponding author upon reasonable request. The author's contact information: wanglong@nimte.ac.cn (L.W.), wgzheng@nimte.ac.cn (W.G.Z.)

ACKNOWLEDGMENTS

This work was financially supported by the National Natural Science Foundation of China (No. 52003280), the Zhejiang Provincial Natural Science Foundation of China (No. LQ21B040003), the S&T Innovation 2025 Major Special Programme of Ningbo (No. 2021Z052), and the Chinese Academy of Sciences Pioneer Hundred Talents Program.

REFERENCES

1 Doroudiani, S.; Park, C. B.; Kortschot, M. T. Processing and characterization of microcellular foamed high-density polythylene/isotactic polypropylene blends. *Polym. Eng. Sci.* **1998**, *38*, 1205–1215.
2 Yang, J.; Xie, J.; Ji, K.; Wang, X.; Jiao, X.; Xu, Z.; Zhao, P.

Microcellular injection molding of polyether-ether-ketone. *Polymer* **2022**, *251*, 124866.
3 Zhao, J.; Zhao, Q.; Wang, C.; Guo, B.; Park, C. B.; Wang, G. High thermal insulation and compressive strength polypropylene foams fabricated by high-pressure foam injection molding and mold opening of nano-fibrillar composites. *Mater. Des.* **2017**, *131*, 1–11.
4 Hou, J.; Zhao, G.; Wang, G.; Dong, G.; Xu, J. A novel gas-assisted microcellular injection molding method for preparing lightweight foams with superior surface appearance and enhanced mechanical performance. *Mater. Des.* **2017**, *127*, 115–125.
5 Wang, G. L.; Zhao, J. C.; Wang, G. Z.; Zhao, H. B.; Lin, J.; Zhao, G. Q.; Park, C. B. Strong and super thermally insulating *in-situ* nanofibrillar PLA/PET composite foam fabricated by high-pressure microcellular injection molding. *Chem. Eng. J.* **2020**, *390*, 124520.
6 Rhim, J. W.; Park, H. M.; Ha, C. S. Bio-nanocomposites for food packaging applications. *Prog. Polym. Sci.* **2013**, *38*, 1629–1652.
7 Ju, Q.; Tang, Z. P.; Shi, H. D.; Zhu, Y. F.; Shen, Y. C.; Wang, T. W. Thermoplastic starch based blends as a highly renewable filament for fused deposition modeling 3D printing. *Int. J. Biol. Macromol.* **2022**, *219*, 175–184.
8 Wang, Y. Y.; Wang, Y.; Zhu, W. B.; Lan, D.; Song, Y. M. Flexible poly(butylene adipate-*co*-butylene terephthalate) enabled high-performance polylactide/wood fiber biocomposite foam. *Ind. Crops Prod.* **2023**, *204*, 117381.
9 Wu, M.; Ren, Q.; Zhu, X.; Li, W.; Luo, H.; Wu, F.; Wang, L.; Zheng, W.; Cui, P.; Yi, X. Super toughened blends of poly(lactic acid) and poly(butylene adipate-*co*-terephthalate) injection-molded foams *via* enhancing interfacial compatibility and cellular structure. *Int. J. Biol. Macromol.* **2023**, *245*, 125490.
10 Zhao, H.; Bian, Y.; Li, Y.; Dong, Q.; Han, C.; Dong, L. Bioresource-based blends of poly(3-hydroxybutyrate-*co*-4-hydroxybutyrate) and stereocomplex polylactide with improved rheological and mechanical properties and enzymatic hydrolysis. *J. Mater. Chem. A* **2014**, *2*, 8881–8892.
11 Najafi, N.; Heuzey, M. C.; Carreau, P. J.; Therriault, D.; Park, C. B. Mechanical and morphological properties of injection molded linear and branched-polylactide (PLA) nanocomposite foams. *Eur. Polym. J.* **2015**, *73*, 455–465.
12 Tang, Y. J.; Wang, Y. Q.; Chen, S. H.; Wang, X. D. Fabrication of low-density poly(lactic acid) microcellular foam by self-assembly crystallization nucleating agent. *Polym. Degrad. Stabil.* **2022**, *198*, 109891.
13 Wang, L.; Hikima, Y.; Ishihara, S.; Ohshima, M. Fabrication of lightweight microcellular foams in injection-molded polypropylene using the synergy of long-chain branches and crystal nucleating agents. *Polymer* **2017**, *128*, 119–127.
14 Ren, Q.; Wu, M. H.; Wang, L.; Zheng, W. E.; Hikima, Y.; Semba, T.; Ohshima, M. Light and strong poly(lactic acid)/cellulose nanofiber nanocomposite foams with enhanced rheological and crystallization property. *J. Supercrit. Fluids* **2022**, *190*, 105758.
15 Ren, Q.; Wu, M. H.; Wang, L.; Zheng, W. E.; Hikima, Y.; Semba, T.; Ohshima, M. Cellulose nanofiber reinforced poly(lactic acid) with enhanced rheology, crystallization and foaming ability. *Carbohydr. Polym.* **2022**, *286*, 119320.
16 Zhu, X.; Ren, Q.; Li, W.; Wu, M.; Weng, Z.; Wang, J.; Zheng, W.; Wang, L. In situ nanofibrillar fully-biobased poly(lactic acid)/poly(ethylene 2,5-furandicarboxylate) composites with promoted crystallization kinetics, mechanical properties, and heat resistance. *Polym. Degrad. Stabil.* **2022**, *206*, 110172.
17 Wang, Y.; Guo, F. M.; Liao, X.; Li, S. J.; Yan, Z. H.; Zou, F. F.; Peng, Q. Y.; Li, G. X. High-expansion-ratio PLLA/PDLA/HNT composite foams with good thermally insulating property and enhanced compression performance *via* supercritical CO_2. *Int. J. Biol. Macromol.* **2023**, *236*, 123961.
18 Liao, X.; Nawaby, A. V.; Naguib, H. E. Porous poly(lactic acid) and PLA-nanocomposite structures. *J. Appl. Polym. Sci.* **2012**, *124*, 585–594.
19 Wu, Y.; Zhang, S.; Han, S. Q.; Yu, K. S.; Wang, L. Y. Regulating cell morphology of poly(lactic acid) foams from microcellular to nanocellular by crystal nucleating agent. *Polym. Degrad. Stabil.* **2022**, *204*, 110117.
20 Jain, S.; Misra, M.; Mohanty, A. K.; Ghosh, A. K. Thermal, mechanical and rheological behavior of poly(lactic acid)/talc composites. *J. Polym. Environ.* **2012**, *20*, 1027–1037.
21 Piekarska, K.; Sowinski, P.; Piorkowska, E.; Ul Haque, M. M.; Pracella, M. Structure and properties of hybrid PLA nanocomposites with inorganic nanofillers and cellulose fibers. *Compos. Part A: Appl. Sci. Manuf.* **2016**, *82*, 34–41.
22 Girdthep, S.; Limwanich, W.; Punyodom, W. Non-isothermal cold crystallization, melting, and moisture barrier properties of silver-loaded kaolinite filled poly(lactic acid) films. *Mater. Chem. Phys.* **2022**, *276*, 125227.
23 Ouchiar, S.; Stoclet, G.; Cabaret, C.; Georges, E.; Smith, A.; Martias, C.; Addad, A.; Gloaguen, V. Comparison of the influence of talc and kaolinite as inorganic fillers on morphology, structure and thermomechanical properties of polylactide based composites. *Appl. Clay Sci.* **2015**, *116*, 231–240.
24 Clarkson, C. M.; Azrak, S. M. E.; Schueneman, G. T.; Snyder, J. F.; Youngblood, J. P. Crystallization kinetics and morphology of small concentrations of cellulose nanofibrils (CNFs) and cellulose nanocrystals (CNCs) melt-compounded into poly(lactic acid) (PLA) with plasticizer. *Polymer* **2020**, *187*, 122101.
25 Zhang, Y. C.; Duvigneau, J.; Sui, X. F.; Vancso, G. J. Foaming of polylactic acid/cellulose nanocrystal composites: pickering emulsion templating for high-homogeneity filler dispersions. *ACS Appl. Polym. Mater.* **2022**, *4*, 111–120.
26 Soleimanpour, A.; Khonakdar, H.; Mousavi, S. R.; Hemmati, F.; Arjmand, M.; Arnhold, K.; Reuter, U.; Khonakdar, H. A. Dynamic crystallization kinetics and morphology of carbonaceous nanofillers-reinforced poly(lactic acid) foams. *Thermochim. Acta* **2022**, *716*, 179308.
27 Kim, S. Y.; Shin, K. S.; Lee, S. H.; Kim, K. W.; Youn, J. R. Unique crystallization behavior of multi-walled carbon nanotube filled poly(lactic acid). *Fibers Polym.* **2010**, *11*, 1018–1023.
28 Ren, Q.; Li, W.; Cui, S.; Ma, W.; Zhu, X.; Wu, M.; Wang, L.; Zheng, W.; Semba, T.; Ohshima, M. Improved thermal insulation and compressive property of bimodal poly(lactic acid)/cellulose nanocomposite foams. *Carbohydr. Polym.* **2023**, *302*, 120419.
29 Nam, J. Y.; Okamoto, M.; Okamoto, H.; Nakano, M.; Usuki, A.; Matsuda, M. Morphology and crystallization kinetics in a mixture of low-molecular weight aliphatic amide and polylactide. *Polymer* **2006**, *47*, 1340–1347.
30 Niu, D.; Shen, T.; Xu, P.; Yu, M.; Liu, T.; Yang, W.; Wang, Z.; Ma, P. Enhanced crystallization, heat resistance and transparency of poly(lactic acid) with self-assembling bis-amide nucleator. *Int. J. Biol. Macromol.* **2023**, *234*, 123584.
31 Bai, H.; Huang, C.; Xiu, H.; Zhang, Q.; Fu, Q. Enhancing mechanical performance of polylactide by tailoring crystal morphology and lamellae orientation with the aid of nucleating agent. *Polymer* **2014**, *55*, 6924–6934.
32 Gao, X.; Qi, S.; Yang, B.; Su, Y.; Li, J.; Wang, D. Synergistic effect of plasticizer and nucleating agent on crystallization behavior of polylactide during fused filament fabrication. *Polymer* **2021**, *215*, 123426.
33 Tang, Y. J.; Li, Z. L.; Chen, S. H.; Wang, X. D. The synergistic effect of polytetrafluoroethylene *in-situ* fibrillation and dibenzoyl sebacate hydrazide on the crystallization and foaming behavior

of poly(lactic acid). *Int. J. Biol. Macromol.* **2022**, *221*, 523–535.
34 Zhao, X.; Yu, J.; Liang, X.; Huang, Z.; Li, J.; Peng, S. Crystallization behaviors regulations and mechanical performances enhancement approaches of polylactic acid (PLA) biodegradable materials modified by organic nucleating agents. *Int. J. Biol. Macromol.* **2023**, *233*, 123581.
35 Xu, T.; Zhang, A.; Zhao, Y.; Han, Z.; Xue, L. Crystallization kinetics and morphology of biodegradable poly(lactic acid) with a hydrazide nucleating agent. *Polym. Test.* **2015**, *45*, 101–106.
36 Li, C. H.; Luo, S. S.; Wang, J. F.; Wu, H.; Guo, S. Y.; Zhang, X. Conformational regulation and crystalline manipulation of PLLA through a self-assembly nucleator. *Biomacromolecules* **2017**, *18*, 1440–1448.
37 Wang, L.; Ando, M.; Kubota, M.; Ishihara, S.; Hikima, Y.; Ohshima, M.; Sekiguchi, T.; Sato, A.; Yano, H. Effects of hydrophobic-modified cellulose nanofibers (CNFs) on cell morphology and mechanical properties of high void fraction polypropylene nanocomposite foams. *Compos. Part A: Appl. Sci. Manuf.* **2017**, *98*, 166–173.
38 Luo, F.; Geng, C.; Wang, K.; Deng, H.; Chen, F.; Fu, Q.; Na, B. New understanding in tuning toughness of β-polypropylene: the role of β-nucleated crystalline morphology. *Macromolecules* **2009**, *42*, 9325–9331.
39 Bai, H.; Zhang, W.; Deng, H.; Zhang, Q.; Fu, Q. Control of crystal morphology in poly(l-lactide) by adding nucleating agent. *Macromolecules* **2011**, *44*, 1233–1237.
40 Leung, S. N.; Park, C. B.; Xu, D.; Li, H.; Fenton, R. G. Computer simulation of bubble-growth phenomena in foaming. *Ind. Eng. Chem. Res.* **2006**, *45*, 7823–7831.
41 Wang, C.; Shaayegan, V.; Ataei, M.; Costa, F.; Han, S.; Bussmann, M.; Park, C. B. Accurate theoretical modeling of cell growth by comparing with visualized data in high-pressure foam injection molding. *Eur. Polym. J.* **2019**, *119*, 189–199.
42 Lin, H.; Chen, Y.; Gao, X. R.; Xu, L.; Lei, J.; Zhong, G. J.; Li, Z. M. Transparent, heat-resistant, ductile, and self-reinforced polylactide through simultaneous formation of nanocrystals and an oriented amorphous phase. *Macromolecules* **2023**, *56*, 2454–2464.
43 Ding, W. D.; Jahani, D.; Chang, E.; Alemdar, A.; Park, C. B.; Sain, M. Development of PLA/cellulosic fiber composite foams using injection molding: crystallization and foaming behaviors. *Compos. Part A Appl. Sci. Manuf.* **2016**, *83*, 130–139.
44 Péter, T.; Litauszki, K.; Kmetty, Á. Improving the heat deflection temperature of poly(lactic acid) foams by annealing. *Polym. Degrad. Stab.* **2021**, *190*, 109646.
45 Tábi, T.; Hajba, S.; Kovács, J. G. Effect of crystalline forms (α' and α) of poly(lactic acid) on its mechanical, thermo-mechanical, heat deflection temperature and creep properties. *Eur. Polym. J.* **2016**, *82*, 232–243.
46 Chai, J. L.; Wang, G. L.; Zhang, A. M.; Li, S.; Zhao, J. C.; Zhao, G. Q.; Park, C. B. Ultra-ductile and strong *in-situ* fibrillated PLA/PTFE nanocomposites with outstanding heat resistance derived by CO_2 treatment. *Compos. Part A Appl. Sci. Manuf.* **2022**, *155*, 106849.

https://doi.org/10.1007/s10118-024-3088-6